Heliyon 9 (2023) e20181

Contents lists available at ScienceDirect

Heliyon

journal homepage: www.cell.com/heliyon

Long-term, real-time and label-free live cell image processing and analysis based on a combined algorithm of CellPose and watershed segmentation

Jiang Jiang [a,1], Zhikun Zeng [b,1], Jiazhao Xu [b], Wenfang Wang [a], Bowen Shi [a], Lan Zhu [a], Yong Chen [a], Weiwu Yao [c,**], Yujie Wang [b,d,e,***], Huan Zhang [a,*]

[a] Department of Radiology, Ruijin Hospital, Shanghai Jiao Tong University School of Medicine, No. 197, Ruijin Er Road, Shanghai, 200025, China
[b] School of Physics and Astronomy, Shanghai Jiao Tong University, 800 Dong Chuan Road, Shanghai, 200240, China
[c] Department of Imaging, Tongren Hospital, Shanghai Jiao Tong University School of Medicine, No. 1111, Xianxia Road, Shanghai, 200036, China
[d] State Key Laboratory of Geohazard Prevention and Geoenvironment Protection, Chengdu University of Technology, No. 1, Dongsanlu, Erxianqiao, Chengdu, 610059, China
[e] Department of Physics, College of Mathematics and Physics, Chengdu University of Technology, No. 1, Dongsanlu, Erxianqiao, Chengdu, 610059, China

ARTICLE INFO

Keywords:
Long-term
Real-time and label-free live cell image processing
Cell proliferation
Cytotoxicity
Cell movement

ABSTRACT

Developing a rapid and quantitative method to accurately evaluate the physiological abilities of living cells is critical for tumor control. Many experiments have been conducted in the field of biology in an attempt to measure the proliferation and movement abilities of cells, but existing methods cannot provide real-time and objective data for label-free cells. The quantitative imaging technique, including an automatic segmentation algorithm for individual label-free cells, has been a breakthrough in this regard. In this study, we develop a combined automatic image processing algorithm of CellPose and watershed segmentation for the long-term and real-time imaging of label-free cells. This method shows strong reliability in cell identification regardless of cell densities, allowing us to obtain accurate information about the number and proliferation ability of the target cells. Additionally, our results also suggest that this method is a reliable way to assess real-time data on drug cytotoxicity, cell morphology, and cell movement ability.

1. Introduction

One of the major challenges in current medical and clinical research is the development of a rapid and quantitative method for

* Corresponding author. Department of Radiology, Ruijin Hospital, Shanghai Jiao Tong University School of Medicine, No. 197, Ruijin Er Road, Shanghai, 200025, China.
** Corresponding author. Department of Imaging, Tongren Hospital, Shanghai Jiao Tong University School of Medicine, No. 1111, Xianxia Road, Shanghai, 200036, China.
*** Corresponding author. School of Physics and Astronomy, Shanghai Jiao Tong University, 800 Dong Chuan Road, Shanghai 200240, China.
E-mail addresses: jiangjiangzty@163.com (J. Jiang), zzk97115_kenny@sjtu.edu.cn (Z. Zeng), xujiazhao@sjtu.edu.cn (J. Xu), wangwf@sjtu.edu.cn (W. Wang), shibowen0525@163.com (B. Shi), Lennon1208@163.com (L. Zhu), shaoer.cy@gmail.com (Y. Chen), yaoweiwuhuan@163.com (W. Yao), yujiewang@sjtu.edu.cn (Y. Wang), huanzhangy@163.com (H. Zhang).
[1] These authors contributed equally to this work and share first authorship.

https://doi.org/10.1016/j.heliyon.2023.e20181
Received 21 May 2023; Received in revised form 6 September 2023; Accepted 13 September 2023
Available online 15 September 2023

evaluating the physiological properties of cells, including their proliferation and migration ability [1,2]. Conventional evaluation methods for cellular physiological states are mainly based on biochemistry assays, which belong to end-point detection [3–5]. Since cells are killed and their structures are destroyed during these detection methods, the true properties of the living cells cannot be reflected directly and accurately [5]. Moreover, these methods cannot meet the needs of high-throughput data analysis because of the cumbersome relevant statistical analysis [6]. In order to solve these problems, researchers have proposed a new approach that can provide detailed information on the entire lifecycle of cells by observing and tracking them in real-time and in situ [7–9]. This method not only greatly deepens our understanding of the physiological properties of cells but can also accelerate drug development processes as it allows us to assess drug cytotoxicity directly and rapidly [3].

Quantitative imaging offers magnificent spatial and temporal resolutions in the measurement of biological phenomena, especially in two-dimensional (2D) cell monolayer models, and it now being widely used in both cell biology and biomedical research [6]. Quantitative imaging allows one to observe the core physiological properties of cells, e.g., cell proliferation, morphology, and migration, at a single-cell level during the cell culture process and therefore to quantify the influence of the external interventions [6,10,11]. Nevertheless, quantitative imaging analysis relies heavily on corresponding recognition and segmentation algorithms, which are usually based on fluorescent labels such as fluorescent proteins and fluorescein in images [12]. However, mounting evidence indicates that the use of fluorescent sensors alters biological responses by affecting the cells' physiological properties [13]. Specifically, the fluorescent proteins have been reported to correlate with the increased cell mortality [14], reactive oxygen species accumulation, and the mitotic arrest [15]; the interruption of critical cell signaling pathways [16]; and the impairment of actin–myosin interactions [17]. Therefore, it is highly crucial to develop a quantitative analysis for label-free cell imaging in order to avoid these shortcomings and obtain more reliable results in the observation of cellular physiological states for future research [6,10].

The first prerequisite of establishing a quantitative analysis method for the long-term and real-time imaging of label-free living cells is to segment the cells accurately [18]. However, the various shapes of cells and their continuous morphology changes during the imaging process present major challenges for the corresponding segmentation algorithms in quantitative analysis [19]. There have been a variety of segmentation algorithms developed for images of label-free cells, including watershed segmentation method [20], edge recognition [21], deep learning algorithms [22], etc. The watershed algorithm is one of the classical segmentation methods used for imaging processing, in which different cells can be found according to their gray level [23–25]. However, segmentation by the watershed algorithm is affected by many errors, especially for images in brightfield mode with low contrast, and cannot meet the high requirements of quantitative experiments. On the other hand, deep learning methods, i.e., the convolutional neural network (CNN) algorithm, are widely applicated in quantitative imaging due to their excellent recognition and great universality [26,27]. Nevertheless, the high-quality training datasets including a wide variety of unlabeled objects are critical to obtain well-segmented results in image processing [28]. The dataset of the LIVECell algorithm released by Christopher Edlund et al. includes 1.6 million cells of 8 different types and the algorithm shows good segmentation ability at the early seeding [6]. The CellPose algorithm has been trained on datasets of about 70,000 segmented objects, mainly including images of fluorescent-labeled cells with few images in brightfield modes [10]. However, there are still some cells that cannot be identified by CNN methods, especially for cells growing to confluence, and in some cases, even only 30% of cells can be found in the images. This suggests the necessity of building a better training dataset with a wider range of cell morphology.

Furthermore, The cell segmentation algorithms primarily on morphological characteristics. Under the influence of pharmaceutical agents, these characteristics often manifest discernible alterations. Hence, the applicability of segmentation algorithms in analyzing the dynamic responses of cells under distinct drug conditions is of paramount significance. In clinical contexts, cisplatin is one of the commonly used drugs for gastric cancer chemotherapy and has shown definite efficacy against gastric cancer by interfering with DNA replication and transcription processes. Currently, there are two common administration methods, transient high-concentration administration and continuous low-concentration administration, for this drug. The direct discernment of disparities between these two modes of administration remains a pivotal focus of current investigation, facilitated through quantitative image analysis methodologies.

In this study, we combined a deep learning algorithm with the watershed segmentation method to segment approximately 21,600,000 label-free BGC-823 and MGC-803 cells in about 55,000 images. We explored cell proliferative ability, morphological characteristics, and movement ability under drug treatment. The results obtained from different analyses are consistent with each other, which verifies the reliability of our algorithm.

2. Materials and methods

2.1. Cell culture and CCK-8 assay

BGC-823 and MGC-803 cell lines used in this experiment were obtained from the Shanghai Institute of Digestive Surgery, Ruijin Hospital, Shanghai Jiao Tong University. The cells were initially cultured in Dulbecco's Modified Eagle Medium (DMEM) (Dalian Meilun Biotechnology Co. LTD) supplemented with 10% fetal bovine serum (FBS) and 1% penicillin-streptomycin (YEASEN Biotech Co. Ltd) at 37 °C with 5% CO_2. Approximately 10,000 cells of each type were seeded onto 96-well plates and incubated in a cell incubator for 24 h. The BGC-823 cells were treated with varying concentrations of cisplatin (0, 10, 20, and 40 μg/mL) for a duration of 2 h. Subsequently, the cells underwent two cycles of Phosphate-Buffered Saline (PBS) washing to eliminate the cisplatin-containing medium, and then cultured in fresh medium for an additional 24 h before conducting the CCK-8 assay. The control group was treated with 0 μg/mL cisplatin, while the experimental groups were exposed to concentrations of 10, 20, and 40 μg/mL groups. As for MGC-803 cells, we adopted a continuous low-dose administration approach, treating the cells with 0, 16, 32, 64, 256, and 512 ng/mL

of cisplatin. The control group received no cisplatin (0 μg/mL), whereas the experimental groups were exposed to more concentrations. Unlike BGC-823 cells, the same medium with cisplatin was used for subsequent imaging to evaluate the results of different drug delivery methods. The absorbance value (O.D. (450 nm)) of the CCK-8 solution was detected at 450 nm, measured by a microplate reader (Tecan Sunrise). PBS (Phosphate-Buffered Saline) was used as the vehicle to administer the drugs. For the CCK-8 experiment, 5 independent replicate wells will be set up at each concentration to ensure the accuracy of the experiment. Two-way ANOVA was utilized for the analysis of CCK-8 assays assessing cell viability. For comparisons involving multiple groups, one-way ANOVA was employed. All outcomes were reported as the mean ± standard deviation (SD) derived from triplicate experiments.

Based on the O.D. values obtained from the enzyme-linked immunosorbent assay (ELISA) reader, the drug concentration versus cell viability curves were plotted using GraphPad Prism (version 9.0.0, GraphPad Software, San Diego, California, USA). The drug concentration was plotted on the *x*-axis, and cell viability was plotted on the *y*-axis. By visualizing the curve, the impact of drug concentration on cell viability could be observed. The drug concentration that led to a 50% decrease in cell viability was determined by analyzing the curve, and this point represents the IC50 value. Typically, curve-fitting software, such as logistic regression, is used to calculate the IC50 value from the data. Note that in the current study, the time point for calculating the IC50 is after 48 h of cell culture.

2.2. Laser scanning confocal microscopy (LSCM) imaging

We utilized a laser scanning confocal microscope (CSU–W1) to perform long-term living cell imaging in the brightfield mode. The microscope had a specified magnification of 10 × or 20 × objective. Each imaging field captured an area of approximately 1.2 × 1.5 mm^2 on the dish. Specifically, for BGC-823 cells treated with different concentrations of cisplatin, we randomly selected three non-overlapping imaging fields for each intervention concentration. Consequently, a total of 12 imaging fields of cells were collected to ensure adequate data for subsequent cell segmentation. For MGC-803 cells, 52 imaging fields were chosen for each concentration (0, 4, 16, 64, 128, and 512 ng/mL). The total imaging duration was 60 h for BGC-823 cells, with a time interval of 5 min between two images, and for MGC-803 cells, the total imaging duration was 48 h with a time interval of 30 min between two images.

2.3. Cell doubling time analysis

The cell doubling time is a common measure used to assess the rate of cell proliferation in cell culture experiments. It is typically calculated using the following formula:

$$\tau = (t_2 - t_1)\frac{\log(2)}{\log(N_2/N_1)},$$

where t_1 and t_2 are the time at the start and end of cell counting respectively, and N is the number of cells at the corresponding time point. We perform cell counts at two different time points during the exponential growth phase of the cells to calculate the cell doubling time. By plugging the appropriate values into the formula, we can determine the time how long it takes for the cell population to double. It is essential to ensure that the cells are in the exponential growth phase and that the time points chosen for cell counting accurately represent this phase for accurate doubling time calculations.

2.4. Imaging processing

In this study, we use three algorithms for image processing, they are watershed segmentation algorithm, CellPose deep learning algorithm, and our self-developed algorithm which combines the two methods. Initially, we employed the watershed segmentation algorithm using MATLAB for image processing. Prior to the formal segmentation process, a series of preprocessing steps are applied to the images. Initially, we employed MATLAB's top-hat transformation to ensure uniform brightness by calculating the morphological opening of the image and subtracting the results from the original image. However, since cell brightness is not uniform, in the subsequent step, we utilized MATLAB's built-in adaptive local thresholding to perform binary image conversion. Once this result is obtained, we applied minor standard opening and closing transformations to remove noise from the image. At this stage, a notable challenge arises due to the intricate cellular structures, including distorted boundaries. To address this, we applied more extensive opening and closing transformations to achieve smoother boundaries. Lastly, we utilized the standard marker-based watershed segmentation algorithm provided by MATLAB to segment the cells. When employing the Cellpose method as the sole labeling technique, we adhered to the developers' established procedure. Initially, we selected a small set of images and manually delineated the shapes and boundaries of cells within these images. In CellPose, the only parameter we need to set is the average diameter of the cell, about 60 pixels. Following the preliminary training of the model, we were able to employ this model to automatically segment a larger number of cells. However, the initial segmentation results often required refinement, necessitating manual adjustments to align the automated labels with the actual cell shapes. This iterative process was repeated approximately 5–6 times, resulting in the development of a robust training model for accurate cell identification. Subsequently, we train a new segmentation model through the standard protocols of CellPose using the extremely huge dataset obtained by watershed segmentation and then apply this model to process all the images. For cells that were not adequately segmented, mainly due to their complex morphology, we further processed the remaining regions using the watershed algorithm after removing the segmented cells.

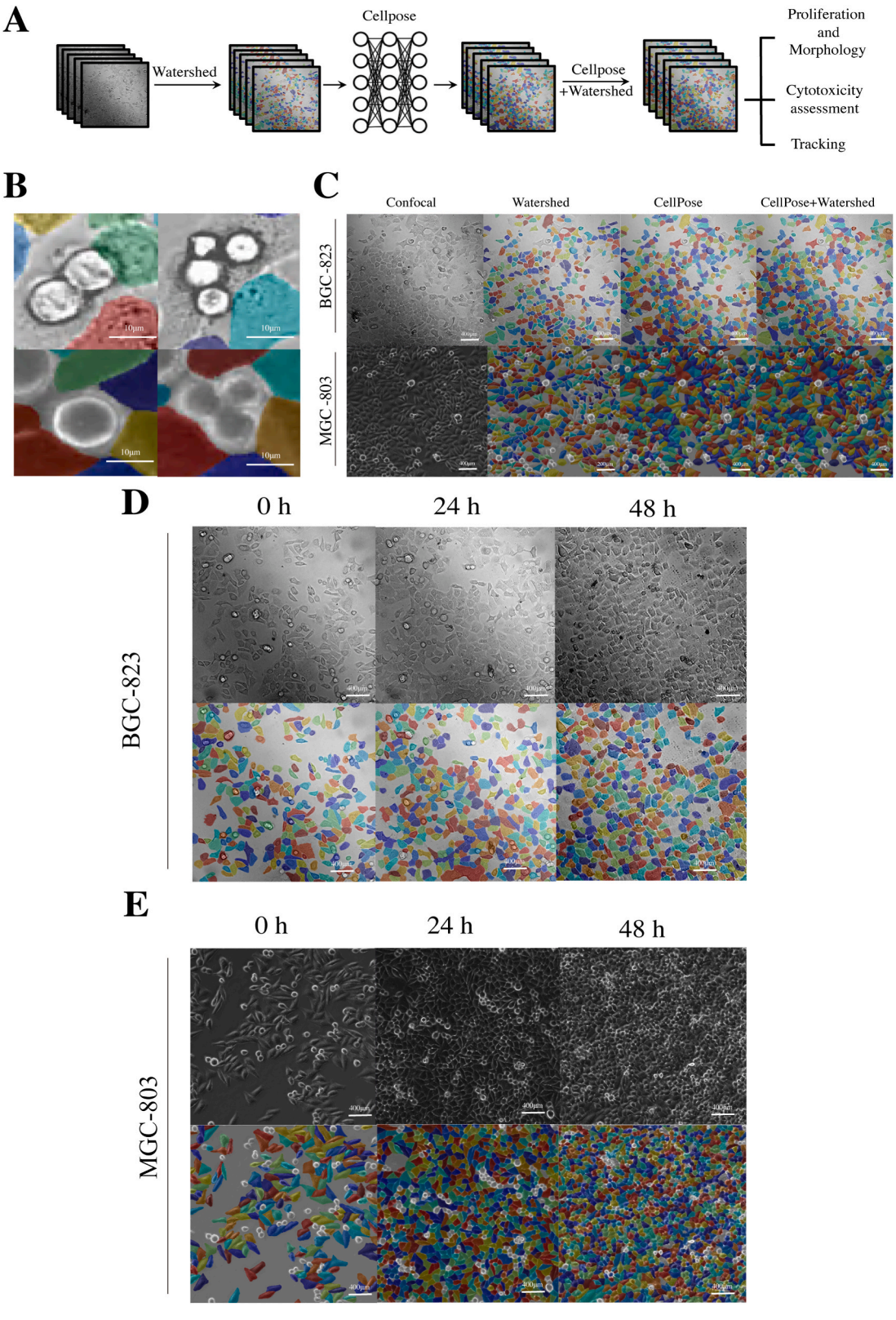

(caption on next page)

Fig. 1. Combined CellPose and watershed segmentation algorithm for long-term, real-time imaging of label-free cells. A. Schematic of the workflow of the combined deep learning and watershed segmentation algorithm for cell image processing. B. The respective segmentation results obtained by the watershed segmentation algorithm, CellPose and our combined algorithm. C. The cells in the division process have brighter bodies with more distinct black edges in ROI. D and E. The confocal images of label-free images and the corresponding segmentation results of the combined algorithm for BGC-823 and MGC-803 cells in different time points (t = 0, 24, 48 h).

3. Results

3.1. Combined CellPose and watershed segmentation algorithm for long-term, real-time imaging of label-free cells

In this study, we combined a deep learning algorithm and the watershed segmentation method to accurately and rapidly segment about 21,600,000 label-free BGC-823 and MGC-803 cells in approximately 55,000 images (Fig. 1A). Before completing the imaging processing and cell segmentation, we observed that a few cells undergoing division appeared brighter with a more distinct black edge (Fig. 1B and see more details in Supplementary S1). This distinct morphological difference arises because these cells moved away from the bottom surface of the medium and into an upper layer during the division process. Note that we did not include these cells in our cell counting or analysis since these morphological differences are not primarily indicative of changes in the physiological properties of the cells themselves. By excluding these cells from our analysis, the remaining cells are representative of their physiological state and facilitate more accurate and reliable quantitative analyses of the cell population under study.

To quantify the accuracy of the segmentation at different cell densities, we compared the number of cells identified by our segmentation program with that of manual marking at different time points. In the manual marking method, we printed the cellular images, and a red dot was utilized to indicate each enumerated cell until all cells in the image were marked. We recorded the number of cells that had been marked, ensuring a comprehensive cell count. The manual detection was performed by two researchers, each repeating the process twice to ensure consistency. In the subsequent analysis of the accurate identification rates, we randomly selected 5 images at each time point (0, 24, 48 h) for two types of cell and three segmentation algorithms, totaling 90 marking results for 30 images. Initially, we can carry out the in-house watershed segmentation program of MATLAB to segment different cells, and about 1,400,000 BGC-823 cells in 8640 images, and about 7,000,000 MGC-803 cells in 18,655 images are initially labeled. However, due to the high noise and low contrast in label-free images, only about 80% of the cells could be well segmented using the watershed algorithm alone (Fig. 1C). To improve the segmentation of cells with complex morphology, we employed the CellPose deep learning algorithm, which significantly enhanced cell segmentation, identifying more than 92% of cells in the region of interest (ROI) (Fig. 1C). Subsequently, we train a new segmentation model through the standard protocols of CellPose using the extremely huge dataset obtained by watershed segmentation, and then apply this model to process all the images (Fig. 1C). The CNN algorithm can not only find those cells that have been labeled by watershed segmentation, proving the reliability of our model but also identify many new cells. In fact, the shapes and coordinates of more than 92% of the cells in the ROI can be obtained through this method, leaving about 8% of the cells unidentified. For cells that were not adequately segmented, mainly due to their complex morphology, we further processed the remaining regions using the watershed algorithm after removing the segmented cells. This additional step resulted in the successful segmentation of more than 95% of the cells (Fig. 1C). As a result, we could accurately identify about 1,600,000 BGC-823 cells in 8640 images and about 20,000,000 MGC-803 cells in 47,320 images using our combined algorithm.

Since it is difficult to display the results of all segmentation results simultaneously, we selected 1 image of each time point and cell type as examples (Fig. 1D and E) to provide further evidence and listed the counting results of different detection methods in Table 1. Note that the reported standard deviation (SD) was obtained through four independent manual detections while the automatic combined segmentation algorithm always got the same counting number. In actuality, we perceive that the standard error of the automated algorithm is the distinction between the automated algorithm and human counting, which is approximately within 10 counts. This high accuracy and reliability make our algorithm well-suited for subsequent quantitative statistical analyses of real-time living cell images.

Additionally, we applied the transient high-concentration of cisplatin to BGC-823 cells and the continuous low-concentration to MGC-803 cells, providing data on cell morphology changes at different rates. This approach allowed us to obtain precise segmentation results under distinct drug conditions, showcasing the sensitivity and accuracy of our algorithm in capturing cell morphology changes. During the course of cell culture with cisplatin, the cells gradually underwent cell death. For simplicity and quantitative analysis, we classified cells as either living or dying based on their morphological and luminance differences, without considering intermediate states (Fig. 2A and B). Dying cells initially underwent shrinkage, leading to a significant decrease in their area (S). As the cell death process continued, the dying cells further disintegrated into smaller fragments, signifying the loss of normal form and the cell shrinkage process, a well-described phenomenon in biology. The probability distribution function (PDF) of the area of all cells,

Table 1
The number of cells in Fig. 1D and E obtained from automatic vs. manual detection.

Cell Type	BGC-823			MGC-803		
Time/h	0	24	48	0	24	48
Automatic Segmentation Algorithm	208	323	650	112	505	836
Manual Detection ± SD	211 ± 1	325 ± 1	660 ± 4	115 ± 0	517 ± 2	843 ± 4
Accurate Identification Rate	98.6 ± 0.5%	99.4 ± 0.3%	98.5 ± 0.6%	97.4 ± 0%	97.7 ± 0.4%	99.2 ± 0.5%

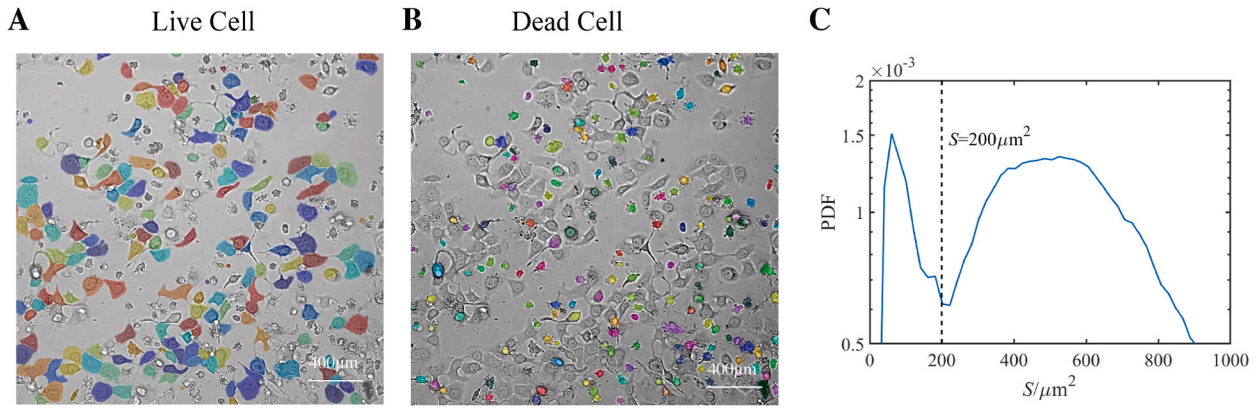

Fig. 2. Living and dying cells identification. A and B. The labeled images of (A) living and (B) dying cells in which we distinguish them by their morphological and luminance differences. C. The probability distribution function (PDF) of cell area obtained from about 4000 images containing both living and dying cells. The dashed line is the threshold of the area $S = 200\ \mu m^2$ between living and dying cells obtained by dividing the two peaks.

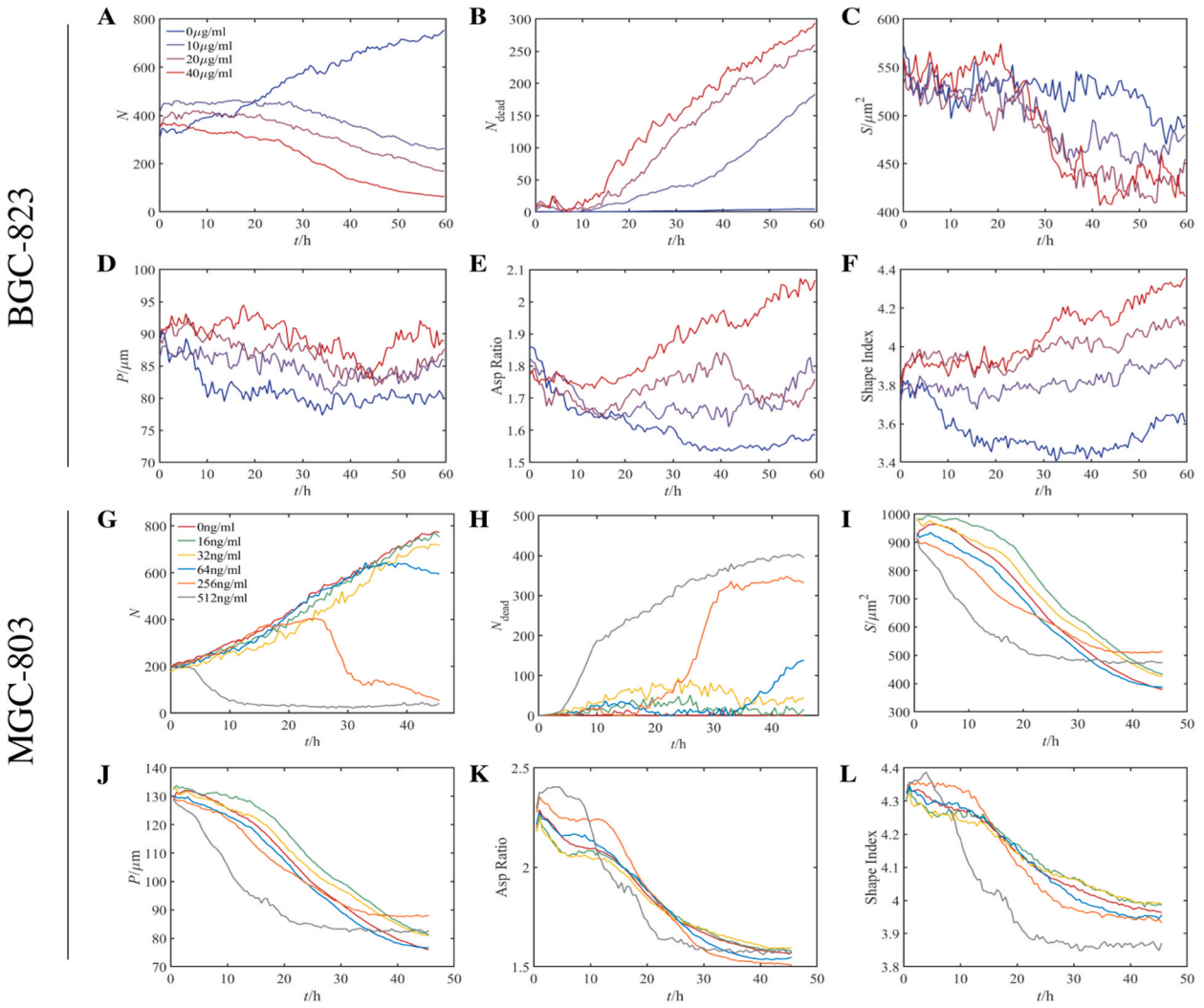

Fig. 3. Cell proliferation and cytotoxicity assessment. A-F and G-L show the counting number, averaged area, perimeter, aspect ratio and shape index of living and dying cells for the BGC-823 and MGC-803 cells, respectively.

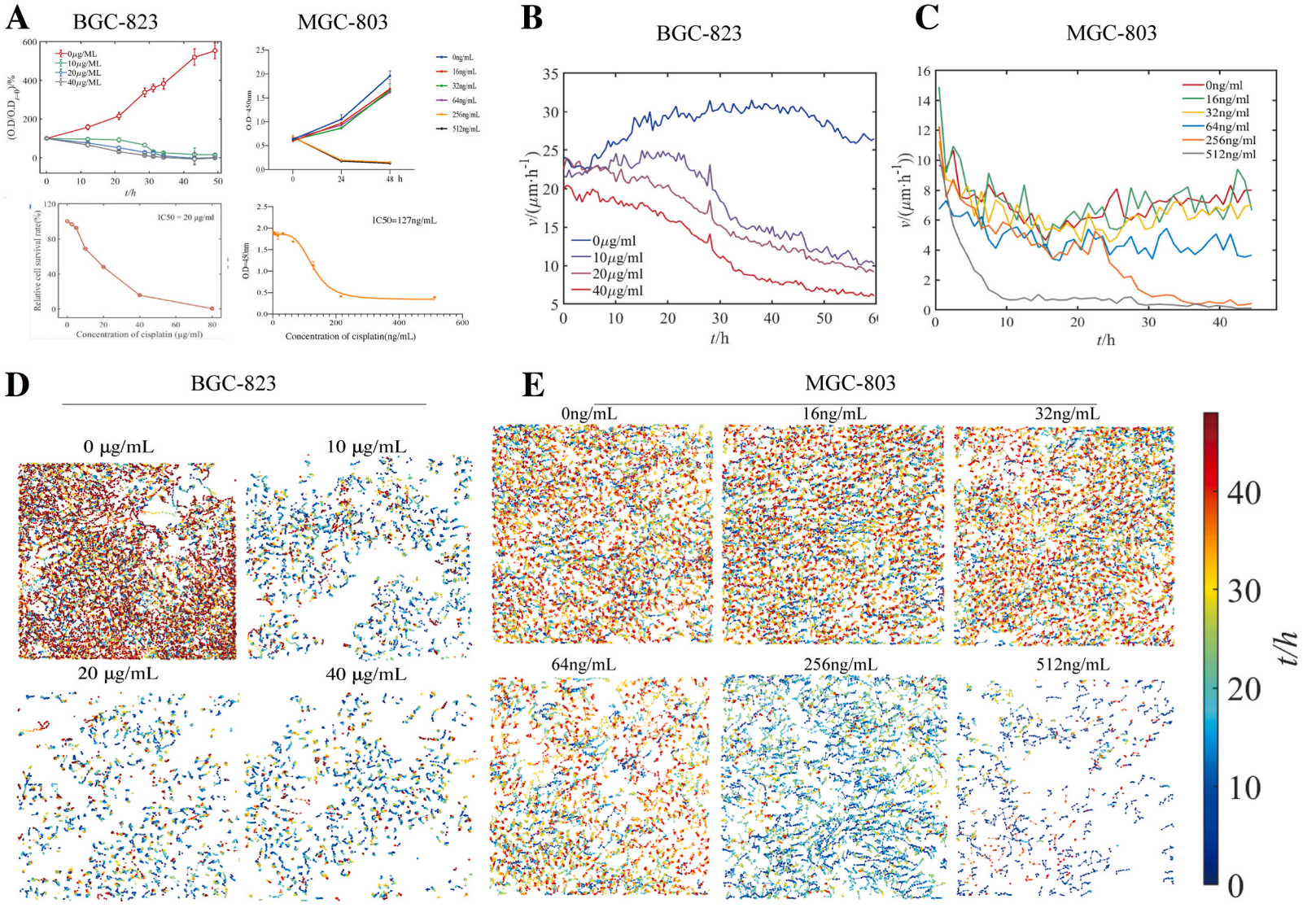

Fig. 4. Long-term, real-time dynamic analysis. A. The O.D. value and IC50 obtained from the CCK-8 assay of BGC-823 cells and MGC-803 cells. B and C. The average speeds of living cells under different concentrations of cisplatin for BGC-853 and MGC-803 cells respectively. D and E. The trajectories of cells under different cisplatin concentrations for BGC-853 and MGC-803 cells respectively.

including both live and dead cells, is presented as a bimodal Gaussian distribution (Fig. 2C). To distinguish living and dying cells effectively, We identified the lowest point between the two peaks of this distribution as the threshold $S = 200\ \mu m^2$ for cell recognition. This approach enabled us to accurately differentiate between cells undergoing the cell death process and those remaining viable, facilitating a comprehensive analysis of cisplatin's impact on cell morphology and survival. Note that the distribution was obtained from approximately 400,000 BGC-823 cells from 2160 images in three realizations, and about 600,000 MGC-803 cells from 2275 images in 25 realizations.

3.2. Cell proliferation and morphology

Using the extensive cell tracking and morphology data obtained from the imaging process, which combines watershed segmentation and deep learning algorithms, we conducted a quantitative analysis of long-term, real-time, and label-free cell imaging. To assess the proliferation ability of both BGC-823 and MGC-803 cells, we performed cell count statistics. Fig. 3A,B,G and H display the number of living and dying cells for the two types of cells, respectively, revealing their respective doubling times to be approximately 36 h for BGC-823 cells and 18 h for MGC-803 cells.

Cell morphology is a crucial parameter for evaluating the health status of cells, as it is closely related to embryonic development, wound healing, and the process of tumor metastasis [29]. Regularly inspecting cell morphology during the culture process helps in identifying signs of contamination, nutritional status, and cell degeneration at an early stage. This continuously changing cell shapes present a challenge for systematic morphological studies. In this experiment, we obtain cell morphology through the imaging process and calculate morphological parameters, such as the averaged cell area (S), perimeter (P), aspect ratio (the ratio $a/\ b$ of the two eigenvalues (a, b) for the equivalent ellipse of the cell) [30], and shape index ($P/\sqrt{S}$) [31] (Fig. 3C–F and 3I-L). In general, the cells will present a more rounded shape with a smaller aspect ratio and shape index when their areas S are the same. Specifically, we find that the BGC-823 cells mainly present an epithelioid shape in the low-density state, while MGC-803 cells tend to grow in a fibroblast-like shape. The shape of cells also varies with the increasing cell density, where elongated cells become shorter and eventually take on an approximate irregular hexagonal shape due to enhanced adhesion between neighboring cells. These results are consistent with the observed reduction in morphological parameters.

3.3. Cytotoxicity assessment

We recorded the number of living cells and the morphological changes in response to different concentrations of cisplatin treatment for both types of cells in Supplementary S2. The results revealed that, under the stimulation of a high concentration of transient cisplatin, the number of BGC-823 cells remained steady in the first 20 h and then decreased at a constant rate thereafter. Beyond a concentration of 10 μg/mL, very few nascent BGC-823 cells were observed (Fig. 3A). This aligns with the findings of the IC50 = 20 μg/mL for BGC-823 cells with culture time of 48 h from the CCK-8 assay (Fig. 4A). Conversely, for concentrations less than 64 ng/mL, the number of MGC-803 cells increased gradually at a similar rate to cells proliferating without cisplatin (Fig. 3G). In the group with a concentration of 256 ng/mL, the cell number remained at about 400 until a large number of cells rapidly died between 24 and 32 h. When the concentration of cisplatin increased to 512 ng/mL, the number of cells remained stable in the first several hours, after which a large number of cells rapidly died. This result is consistent with the IC50 of 127 ng/mL for MGC803 cells. This indicates that cisplatin not only significantly inhibits the proliferation of living cells but also exhibits considerable toxicity to cellular tissues, resulting in a significant reduction in the number of living cells. Moreover, the time point at which a significant decrease in cell numbers occurred was closely correlated with the drug concentration. Higher cisplatin concentrations led to an earlier onset of the decrease in cell numbers [32]. Crumpling and disintegration of cells were also observed at the same time for cells treated with different drug concentrations (Fig. 3C–F and 3I-L). Furthermore, by contrasting the trends in the morphological transformations of the two cell types, we have also discerned that transient administration of elevated concentrations precipitates rapid and marked alterations in cellular morphology, while sustained application of lower concentrations results in a gradual evolution of cell shape over time.

3.4. Long-term, real-time dynamic analysis

In the context of tumor metastasis research, accurately assessing cell movement ability is of paramount importance [33,34]. Recent simulation studies have highlighted the significance of various parameters related to cell movement ability, such as single-cell motile speed, the persistence time of cell tracks, and the target shape index of cell morphology, in governing the jamming transition of bronchial epithelial cells [31]. However, the current lack of image processing technology capable of accurately identifying individual cells often leads to measurement methods that rely on chemical reactions, which can confound the assessment of cells' proliferation and movement abilities. The average speeds and trajectories of cells are crucial parameters that represent the movement ability of cells. Fig. 4B and C shows the average speeds of living cells under different concentrations of cisplatin, which are obtained using the tracking algorithm to assess cell movement ability [35]. We calculated the average speed of cells at different time points. The results show that for the BGC-823 cell treatment group with cisplatin, cell speeds significantly decrease after 24 h of culture, which aligns with the time of decreased cell numbers. Notably, after 34 h of treatment, the curves of cell movement speeds tend to flatten, indicating that most cells in the culture medium have already died. For MGC-803 cells, the average speed of cells remains at a high value at the beginning of the culture but decreases rapidly thereafter. The treatment groups with different concentrations of cisplatin for both cell types exhibit earlier time points at which cell movement speeds start to decrease rapidly, corresponding to the concentration increase of cisplatin,

consistent with the evaluation of cell numbers. The trajectories of cells under different cisplatin concentrations are shown in Fig. 4D and E. The cells in groups with larger cisplatin concentrations move slowly. In addition, the ranges of the cells' movements also gradually become smaller with the increase in the number of cells. This is because when cells undergo a jamming transition, their movements are limited by their neighbors, and the "cage effect" occurs. This result is consistent with the conclusions of previous studies that found that a cell's movement is affected by its neighbors in the confluent tissue, resulting in the cells slowing down and forming a solid-like state [36,37].

4. Discussion

Previous studies have highlighted the importance of both tumor cell proliferation and cell mobility in triggering tumor progression [29]. Therefore, an accurate and real-time assessment of these abilities is crucial for effective tumor control [38,39]. Many experiments have been conducted in the field of biology to measure cell proliferation and movement abilities. However, existing methods often lack the capability to provide real-time and unbiased data for evaluating these abilities without interfering with the cells' physiological state [6]. Moreover, few methods have effectively integrated the measurement of both abilities within a single experiment while maintaining a clear distinction between them. In this study, we have combined long-term living cell imaging technology, image processing technology, and cell trajectory tracking technology to comprehensively assess the proliferation and movement abilities of gastric cancer cells. In typical CNN-based segmentation algorithms, a well-developed training model for new biological image types often requires a large dataset of human-labeled images. In the current study, we leveraged the classical automatic watershed segmentation algorithm to initially label approximately 8,400,000 cells in about 27,000 images, constituting a substantial training dataset. Although not all cells were perfectly segmented, this dataset proved sufficient to train the adaptive segmentation model of the CellPose algorithm using their standard protocol based on these labeled images. It is difficult to obtain such an unprecedented large-scale dataset manually. At the same time, we use the watershed algorithm to make up for the shortcomings of CNN algorithm and further modify the processed images, giving more accurate segmentation results compared to ones obtained by using CNN algorithm alone. This innovative approach allows us to obtain accurate and real-time data for evaluating these critical cell properties, providing valuable insights for tumor control strategies.

The quantitative analysis of long-term, real-time imaging technology for label-free cells has found widespread applications in various biological research fields since its initial development [3]. Image processing technology has been effectively utilized to study cell shape, dynamics, and their relationships, as demonstrated in studies such as the jamming transition of asthma cells [7,31]. In our study, we successfully captured the process of cell division and proliferation over an extended period without interfering with the physiological state of the cells. Utilizing image processing technology, we accurately identified and segmented the cells, allowing us to count the number of cells at different time points. The population doubling time obtained from our image processing approach correlated well with the results of the CCK-8 assay, confirming the reliability of our method. Compared to traditional methods relying on measuring cellular metabolic activity or nucleic acid concentrations, our approach offers more objectivity and convenience in obtaining accurate data. Furthermore, we tracked the trajectories of gastric cancer cells both with and without cisplatin interference in our study. At the initial stage of culture, the average cell speeds slowed down as the cell density increased, reflecting the cellular jamming transition. The cell speeds decreased even more rapidly when exposed to higher concentrations of cisplatin, indicating the impact of the drug on cell movement. Our findings shed light on the dynamic behaviors of cells and their responses to drug intervention, providing valuable insights for tumor control and related research.

Accurately measuring the onset time of anti-tumor drugs for different drug administration methods is indeed a significant challenge in cancer research. Traditional methods, such as setting time gradients *in vitro* experiments, have been employed to explore drug onset time. However, these approaches heavily rely on the experience of the operator, leading to low repeatability and potential bias in the results [7]. In this study, we use cisplatin to interfere in the proliferation of BGC-823 and MGC-803 cells. The results show that for different drug administration methods, the number of cells does not change significantly within the first hours (see Supplementary S3 for more detailed results). After a concentration-dependent time point, most cells start to retract and leave the culture dish, resulting in a decrease in the number of living cells. We also observed that the transient high-concentration administration led to rapid and significant changes in cell morphology, while the continuous low-concentration administration resulted in gradual morphological changes over time *in vitro*. Overall, our experimental design and cell segmentation algorithm allowed us to investigate the effects of cisplatin under different drug administration methods, providing valuable insights into its antitumor mechanisms and potential therapeutic applications. Compared with other chemical evaluation methods, this method can identify the onset time of the drugs directly and save a lot of time and cost [40]. Additionally, this method demonstrates high repeatability and places minimal demands on the experimenter's expertise, as it relies on automated image processing technology for data analysis. Furthermore, by using image processing technology, our method avoids the potential negative impacts on operators associated with other biological evaluation methods that involve the use of highly carcinogenic reagents or toxic substances.

In summary, the comprehensive application of long-term and real-time imaging technology to label-free cells, combined with an automatic image processing algorithm, proves to be an effective and user-friendly method to assess crucial physiological properties of cells, such as their proliferation ability, morphological characteristics, and movement ability. The ease of use and high repeatability make this approach valuable for various research applications. However, there are still certain limitations in the algorithm. Due to the necessity for subtle parameter adjustments of the watershed segmentation algorithm when applied to different cell types, the performance of this program tends to be less optimal in addressing novel cell instances. Furthermore, with undergoing two rounds of watershed segmentation and one round of deep learning algorithm, the computational speed of this approach is comparatively slower compared to a direct implementation of neural network algorithms. On the other hand, we focused on exploring this method with a

preliminary experiment using gastric cancer cells (BGC-823 and MGC-803 cells). It is essential to acknowledge that tumor control is a multifaceted challenge, involving numerous factors, such as tumor cell activity, the tumor microenvironment, immune response, and drug metabolism [41–43]. While our *in vitro* experiments provided valuable insights and data on cellular properties, *in vivo* experiments remain the most conclusive evidence for validating the responses of cells in a realistic biological context. In this preliminary exploration, we limited our study to *in vitro* experiments due to the technical complexity of *in vivo* imaging experiments. However, the results obtained from our study are critical for predicting real-world biological processes and can pave the way for further research. In future studies, we plan to conduct *in vivo* experiments, such as organoid experiments, involving more cell types, and provide real-time and reliable data to advance our understanding of tumor metastasis and aid in the development of anti-tumor drugs. By expanding our research and incorporating more advanced methodologies, we aim to gain a comprehensive understanding of cellular behavior and contribute significantly to cancer research and therapeutic strategies.

5. Conclusion

This study addresses a critical need in tumor control by developing a rapid and quantitative method to evaluate living cell physiology accurately. Our innovative approach combines automatic image processing algorithms, CellPose, and watershed segmentation, enabling real-time imaging of label-free cells with high reliability. This method provides precise data on cell proliferation and movement abilities, drug cytotoxicity, and cell morphology. We hope this work inspires further research to advance tumor control and benefit patients.

Author contributions

Yujie Wang; Weiwu Yao; Huan Zhang: Conceived and designed the experiments; Contributed reagents, materials, analysis tools or data. Jiang Jiang: Performed the experiments; Wrote the paper. Jiazhao Xu; Wenfang Wang; Bowen Shi: Performed the experiments. Zhikun Zheng: Performed the experiments; Analyzed and interpreted the data; Wrote the paper. Jiazhao Xu; Yong Chen: Analyzed and interpreted the data. Lan Zhu: Contributed reagents, materials, analysis tools or data; Wrote the paper.

Data availability statement

Data will be made available on request.

Funding

This study was supported by grants from the National Natural Sciences Foundation of China (No. 82271934 and No. 11974240), the Science and Technology Commission of Shanghai Municipality (No. 22YF1419900), and Medical Engineering Cross Research Foundation of Shanghai Jiao Tong University (No. ZH2018QNA52 and No. YG2021QN08).

Declaration of competing interest

The authors declare no conflict of interest.

Acknowledgements

We would like to express our gratitude to Ying Huang and all members of the Core Facility of Basic Medical Sciences at Shanghai Jiao Tong University for their valuable technical support throughout this study. Their expertise and assistance have been instrumental in the successful execution of our research.

Appendix A. Supplementary data

Supplementary data to this article can be found online at https://doi.org/10.1016/j.heliyon.2023.e20181.

References

[1] S. Bormans, G. Oudebrouckx, P. Vandormael, T. Vandenryt, P. Wagner, V. Somers, R. Thoelen, Pulsed thermal method for monitoring cell proliferation in real-time, Sensors (2021) 21, https://doi.org/10.3390/s21072440.

[2] R. Parboosing, G. Mzobe, L. Chonco, I. Moodley, Cell-based assays for assessing toxicity, A Basic Guide, MC 13 (2016) 13–21, https://doi.org/10.2174/1573406412666160229150803.

[3] F. Yang, R. Riedel, P. del Pino, B. Pelaz, A.H. Said, M. Soliman, S.R. Pinnapireddy, N. Feliu, W.J. Parak, U. Bakowsky, N. Hampp, Real-time, label-free monitoring of cell viability based on cell adhesion measurements with an atomic force microscope, J. Nanobiotechnol. 15 (2017) 23, https://doi.org/10.1186/s12951-017-0256-7.

[4] A. Adan, Y. Kiraz, Y. Baran, Cell proliferation and cytotoxicity assays, Curr. Pharmaceut. Biotechnol. 17 (2016), https://doi.org/10.2174/1389201017666160808160513.

[5] H. Tahara, S. Matsuda, Y. Yamamoto, H. Yoshizawa, M. Fujita, Y. Katsuoka, T. Kasahara, High-content image analysis (HCIA) assay has the highest correlation with direct counting cell suspension compared to the ATP, WST-8 and Alamar blue assays for measurement of cytotoxicity, J. Pharmacol. Toxicol. Methods 88 (2017), https://doi.org/10.1016/j.vascn.2017.08.003.

[6] C. Edlund, T.R. Jackson, N. Khalid, N. Bevan, T. Dale, A. Dengel, S. Ahmed, J. Trygg, R. Sjögren, LIVECell—a large-scale dataset for label-free live cell segmentation, Nat. Methods 18 (2021) 1038–1045, https://doi.org/10.1038/s41592-021-01249-6.

[7] L. Cai, X. Qin, Z. Xu, Y. Song, H. Jiang, Y. Wu, H. Ruan, J. Chen, Comparison of cytotoxicity evaluation of anticancer drugs between real-time cell analysis and CCK-8 method, ACS Omega 4 (2019) 12036–12042, https://doi.org/10.1021/acsomega.9b01142.

[8] S.L. Oo, S. Venkatesh, A.-M. Ilyas, V. Karthikeyan, C.M. Arava, E.Y. Kong, C.-C. Yeung, X. Chen, P.K.N. Yu, V.A.L. Roy, Gating a single cell: a label-free and real-time measurement method for cellular progression, Anal. Chem. 92 (2020) 1738–1745, https://doi.org/10.1021/acs.analchem.9b03136.

[9] G. Demirel, F.F.K. Demirsoy, Ö. Irmak, Cytotoxicity evaluation of eluates from universal adhesives by real-time cell analysis, Dent. Mater. J. 39 (2020), https://doi.org/10.4012/dmj.2019-221.

[10] C. Stringer, T. Wang, M. Michaelos, M. Pachitariu, Cellpose: a generalist algorithm for cellular segmentation, Nat. Methods 18 (2021) 100–106, https://doi.org/10.1038/s41592-020-01018-x.

[11] M. Pachitariu, C. Stringer, Cellpose 2.0: how to train your own model, Nat. Methods (2022) 1–8, https://doi.org/10.1038/s41592-022-01663-4.

[12] A. Watakabe, Y. Komatsu, S. Ohsawa, T. Yamamori, Fluorescent in situ hybridization technique for cell type identification and characterization in the central nervous system, Methods (2010) 52, https://doi.org/10.1016/j.ymeth.2010.07.003.

[13] M. Zhao, B. Li, H. Zhang, F. Zhang, Activatable fluorescence sensors for in vivo bio-detection in the second near-infrared window, Chem. Sci. 12 (2021) 3448–3459, https://doi.org/10.1039/D0SC04789A.

[14] H.S. Liu, M.S. Jan, C.K. Chou, P.H. Chen, N.J. Ke, Is green fluorescent protein toxic to the living cells? Biochem. Biophys. Res. Commun. 260 (1999) 6, https://doi.org/10.1006/bbrc.1999.0954.

[15] R. Dixit, R. Cyr, Cell damage and reactive oxygen species production induced by fluorescence microscopy: effect on mitosis and guidelines for non-invasive fluorescence microscopy, Plant J.: Cell. Mol. Biol. (Sarreguemines, Fr., Online) 36 (2003), https://doi.org/10.1046/j.1365-313x.2003.01868.x.

[16] M. Baens, H. Noels, V. Broeckx, S. Hagens, S. Fevery, A.D. Billiau, H. Vankelecom, P. Marynen, The dark side of EGFP: defective polyubiquitination, PLoS One 1 (2006) e54, https://doi.org/10.1371/journal.pone.0000054.

[17] O. Agbulut, C. Coirault, N. Niederländer, A. Huet, P. Vicart, A. Hagège, M. Puceat, P. Menasché, GFP expression in muscle cells impairs actin-myosin interactions: implications for cell therapy, Nat. Methods 3 (2006), https://doi.org/10.1038/nmeth0506-331.

[18] J. Jang, C. Wang, X. Zhang, H.J. Choi, X. Pan, B. Lin, Y. Yu, C. Whittle, M. Ryan, Y. Chen, K. Lee, A deep learning-based segmentation pipeline for profiling cellular morphodynamics using multiple types of live cell microscopy, Cell Reports Methods 1 (2021), 100105, https://doi.org/10.1016/j.crmeth.2021.100105.

[19] Y. Al-Kofahi, A. Zaltsman, R. Graves, W. Marshall, M. Rusu, A deep learning-based algorithm for 2-D cell segmentation in microscopy images, BMC Bioinf. 19 (2018), https://doi.org/10.1186/s12859-018-2375-z.

[20] Y.F. Lin, Y. Diao, Y.Z. Du, J.G. Zhang, L. Li, P.Z. Liu, Automatic Cell Counting for Phase-Contrast Microscopic Images Based on a Combination of Otsu and Watershed Segmentation Method, Microscopy Research and Technique, 2022, p. 85, https://doi.org/10.1002/jemt.23893.

[21] L. Atia, D. Bi, Y. Sharma, J.A. Mitchel, B. Gweon, S.A. Koehler, S.J. DeCamp, B. Lan, J.H. Kim, R. Hirsch, A.F. Pegoraro, K.H. Lee, J.R. Starr, D.A. Weitz, A. C. Martin, J.-A. Park, J.P. Butler, J.J. Fredberg, Geometric constraints during epithelial jamming, Nat. Phys. 14 (2018) 613–620, https://doi.org/10.1038/s41567-018-0089-9.

[22] T. Falk, D. Mai, R. Bensch, Ö. Çiçek, A. Abdulkadir, Y. Marrakchi, A. Böhm, J. Deubner, Z. Jäckel, K. Seiwald, A. Dovzhenko, O. Tietz, C.D. Bosco, S. Walsh, D. Saltukoglu, T.L. Tay, M. Prinz, K.K. Palme, M. Simons, I. Diester, T. Brox, O. Ronneberger, U-Net, Deep learning for cell counting, detection, and morphometry, Nat. Methods 16 (2019), https://doi.org/10.1038/s41592-018-0261-2.

[23] E. Dougherty, S. Beucher, F. Meyer, The Morphological Approach to Segmentation: the Watershed Transformation, 2018, pp. 433–481, https://doi.org/10.1201/9781482277234-12.

[24] L. Najman, M. Couprie, Watershed algorithms and contrast preservation, in: I. Nyström, G. Sanniti di Baja, S. Svensson (Eds.), Discrete Geometry for Computer Imagery, Springer, Berlin, Heidelberg, 2003, pp. 62–71, https://doi.org/10.1007/978-3-540-39966-7_5.

[25] L. Vincent, P. Soille, Watersheds in digital spaces: an efficient algorithm based on immersion simulations, IEEE Trans. Pattern Anal. Mach. Intell. 13 (1991) 583–598, https://doi.org/10.1109/34.87344.

[26] V.V. Da, K. T, L. Km, M. Dn, Q. Nt, D. Mm, M. I, T. Y, A. Ea, C. Mw, Deep learning automates the quantitative analysis of individual cells in live-cell imaging experiments, PLoS Comput. Biol. 12 (2016), https://doi.org/10.1371/journal.pcbi.1005177.

[27] E. Moen, D. Bannon, T. Kudo, W. Graf, M. Covert, D. Van Valen, Deep learning for cellular image analysis, Nat. Methods 16 (2019) 1233–1246, https://doi.org/10.1038/s41592-019-0403-1.

[28] M. Schwendy, R.E. Unger, S.H. Parekh, EVICAN-a balanced dataset for algorithm development in cell and nucleus segmentation, Bioinformatics 36 (2020) 3863–3870, https://doi.org/10.1093/bioinformatics/btaa225.

[29] J. Furkel, M. Knoll, S. Din, N.V. Bogert, T. Seeger, N. Frey, A. Abdollahi, H.A. Katus, M.H. Konstandin, C. More, A high-content single-cell morphology recognition methodology for liquid biopsies toward personalized cardiovascular medicine, Cell Reports Medicine 2 (2021), 100436, https://doi.org/10.1016/j.xcrm.2021.100436.

[30] Z. Mousavikhamene, D.J. Sykora, M. Mrksich, N. Bagheri, Morphological features of single cells enable accurate automated classification of cancer from non-cancer cell lines, Sci. Rep. 11 (2021), 24375, https://doi.org/10.1038/s41598-021-03813-8.

[31] J.A. Park, J.H. Kim, D. Bi, J.A. Mitchel, N.T. Qazvini, K. Tantisira, C.Y. Park, M. McGill, S.-H. Kim, B. Gweon, J. Notbohm, R. Steward Jr., S. Burger, S.H. Randell, A.T. Kho, D.T. Tambe, C. Hardin, S.A. Shore, E. Israel, D.A. Weitz, D.J. Tschumperlin, E.P. Henske, S.T. Weiss, M.L. Manning, J.P. Butler, J.M. Drazen, J. J. Fredberg, Unjamming and cell shape in the asthmatic airway epithelium, Nat. Mater. 14 (2015) 1040–1048, https://doi.org/10.1038/nmat4357.

[32] L.K. Wardhani, W.A. Kentjono, A.C. Romdhoni, Association between dose and duration of cisplatin exposure with cytotoxicity effect on nasopharyngeal carcinoma stem cell, Indian J. Otolaryngol. Head Neck Surg. 71 (2019) 373–377, https://doi.org/10.1007/s12070-018-1317-4.

[33] C.P. McCann, P.W. Kriebel, C.A. Parent, W. Losert, Cell speed, persistence and information transmission during signal relay and collective migration, J. Cell Sci. 123 (2010) 1724–1731, https://doi.org/10.1242/jcs.060137.

[34] O. St, V. Nk, Live cell imaging and analysis to capture T-cell motility in real-time, Methods Mol. Biol. (2019) 1930, https://doi.org/10.1007/978-1-4939-9036-8_5.

[35] J. Jiang, Z.K. Zeng, Z.C. Pan, B.W. Shi, Y.J. Wang, H. Zhang, Collective dynamics of gastric cancer cells in fluid, Phys. Rev. 104 (2021), https://doi.org/10.1103/PhysRevE.104.064402.

[36] X. Yang, D. Bi, M. Czajkowski, M. Merkel, M.L. Manning, M.C. Marchetti, Correlating cell shape and cellular stress in motile confluent tissues, Proc. Natl. Acad. Sci. USA 114 (2017) 12663–12668, https://doi.org/10.1073/pnas.1705921114.

[37] T.E. Angelini, E. Hannezo, X. Trepat, M. Marquez, J.J. Fredberg, D.A. Weitz, Glass-like dynamics of collective cell migration, Proc. Natl. Acad. Sci. USA 108 (2011) 4714–4719, https://doi.org/10.1073/pnas.1010059108.

[38] S. Lebourgeois, A. Fraisse, C. Hennechart-Collette, L. Guillier, S. Perelle, S. Martin-Latil, Development of a real-time cell analysis (rtca) method as a fast and accurate method for detecting infectious particles of the adapted strain of hepatitis A virus, Front. Cell. Infect. Microbiol. 8 (2018) 335, https://doi.org/10.3389/fcimb.2018.00335.

[39] A. Wells, J. Grahovac, S. Wheeler, B. Ma, D. Lauffenburger, Targeting tumor cell motility as a strategy against invasion and metastasis, Trends Pharmacol. Sci. 34 (2013) 283–289, https://doi.org/10.1016/j.tips.2013.03.001.

[40] S. Kamiloglu, G. Sari, T. Ozdal, E. Capanoglu, Guidelines for cell viability assays, Food Frontiers 1 (2020) 332–349, https://doi.org/10.1002/fft2.44.

[4]1 R.J. Sullivan, J.S. Weber, Immune-related toxicities of checkpoint inhibitors: mechanisms and mitigation strategies, Nat. Rev. Drug Discov. 21 (2022) 495–508, https://doi.org/10.1038/s41573-021-00259-5.

[42] J.J. Mao, G.G. Pillai, C.J. Andrade, J.A. Ligibel, P. Basu, L. Cohen, I.A. Khan, K.M. Mustian, R. Puthiyedath, K.S. Dhiman, L. Lao, R. Ghelman, P. Cáceres Guido, G. Lopez, D.F. Gallego-Perez, L.A. Salicrup, Integrative oncology: addressing the global challenges of cancer prevention and treatment, CA A Cancer J. Clin. 72 (2022) 144–164, https://doi.org/10.3322/caac.21706.

[43] X. Lian, K. Yang, R. Li, M. Li, J. Zuo, B. Zheng, W. Wang, P. Wang, S. Zhou, Immunometabolic rewiring in tumorigenesis and anti-tumor immunotherapy, Mol. Cancer 21 (2022) 27, https://doi.org/10.1186/s12943-021-01486-5.